

# Preparation of Sn–Ag–In ternary solder bumps by electroplating in sequence and reliability

Wang Dongliang(王栋良)<sup>1,2</sup>, Yuan Yuan(袁媛)<sup>1</sup>, and Luo Le(罗乐)<sup>1,†</sup>

<sup>1</sup>State Key Laboratory of Transducer Technology, Shanghai Institute of Microsystem and Information Technology, Chinese Academy of Sciences, Shanghai 200050, China

<sup>2</sup>Graduate of University, Chinese Academy of Sciences, Beijing 100049, China

**Abstract:** This paper describes a technique that can obtain ternary Sn–Ag–In solder bumps with fine pitch and homogenous composition distribution. The main feature of this process is that tin–silver and indium are electroplated on copper under bump metallization (UBM) in sequence. After an accurate reflow process, Sn<sub>1.8</sub>Ag<sub>9.4</sub>In solder bumps are obtained. It is found that the intermetallic compounds (IMCs) between Sn–Ag–In solder and Cu grow with the reflow time, which results in an increase in Ag concentration in the solder area. So during solidification, more Ag<sub>2</sub>In nucleates and strengthens the solder.

**Key words:** Sn–Ag–In solder bumps; electroplating; microstructure; shear strength

**DOI:** 10.1088/1674-4926/32/8/083005      **PACC:** 8140

## 1. Introduction

In recent years, the binary lead-free alloy of Sn–Ag has attracted plenty of attention owing to its better mechanical properties and potential replacement of the traditional Sn<sub>37</sub>Pb eutectic solder<sup>[1,2]</sup>. However, the high melting point of Sn<sub>3.5</sub>Ag solder (221 °C) more or less restricts its applications in the electronics industry. An alternative approach is to use ternary solder alloys [Sn–Ag–X (X = In, Bi, Zn, Cu)] with lower melting points and higher shear strengths<sup>[3–6]</sup>. Among them, indium-containing solder shows excellent wettability, ductility, and fatigue resistance, being regarded as a competitive candidate for conjunctive material<sup>[7]</sup>. Although the Sn–Ag–In ternary solder system has been studied for a long time already, research has mostly focused on intermetallic reactions, such as Ag/In, In/Sn, Sn/Ag/Cu/In, and their mechanical properties in bulk material<sup>[8–11]</sup>. Few reports have investigated Sn–Ag–In solder bumps in ball grid array (BGA) applications<sup>[12–14]</sup>. However, these bumps were usually prepared by placing solder balls on pads followed by reflow, and always with large size (400–760 μm in diameter). Therefore it was not appropriate for high density packaging.

Of all those technologies available to manufacture solder bumps, electroplating is by far the most commercially viable process for fine pitch, small size, high yield and volume production<sup>[15–17]</sup>. However, for ternary solder, it is usually difficult to get suitable chemical solutions for electroplating, so for the addition of the desired amount of the third element, it is necessary to modify the present electroplating process.

The present research is motivated by the desire for a feasible electroplating bumping process of Sn–Ag–In ternary solder bumps. The process consists of several steps. However, they can be grouped into three main parts: 1. UBM, 2. bump formation by electroplating and 3. reflow.

## 2. Experimental procedures

As mentioned, the solder bump preparation process is divided into three main phases: UBM, bump formation and reflow. Furthermore, each one of them consists of several steps as well. Figure 1 shows all of the individual steps.

### 2.1. UBM preparation

The substrates used in this study were prepared from blank Si wafers. 5000 Å SiO<sub>2</sub> was formed first by thermal oxidation, then 6000 Å Al was sputtered (Fig. 1(a)), followed by photolithography of 2 μm LC100A (Fig. 1(b)) and erosion to form an Al pad (Fig. 1(c)). 3000 Å SiO<sub>2</sub> was deposited by plasma-enhanced chemical vapor deposition (PECVD) on the substrate (Fig. 1(d)), followed by photolithography of 2.5 μm LC100A (Fig. 1(e)) and ion beam etching (IBE) to form the open window of SiO<sub>2</sub> (Fig. 1(f)). Then 500/2000 Å TiW/Cu was sputtered onto the above substrate (Fig. 1(g)), which played the roles of adhesion to the substrate, barrier to solder diffusion and seed layer for electroplating, respectively. And then photolithography of 30 μm AZ9260 thick photoresist was applied to pattern the area-array solder bumps (Fig. 1(h)). To get 30 μm AZ9260 thick photoresist with good uniformity, the substrate was spun at 600 rpm for 30 s and then horizontally laid for another 10 min. The lithography was carried out on a KarlSuss MA6 with a light intensity of 18 mW/cm<sup>2</sup> for 100 s. The development was processed in a solution of 200 mL AZ400K and 700 mL water for 90 s. Before Cu electroplating, the substrate was treated with plasma to remove the photoresist residue. Afterwards, 5 μm Cu UBM was obtained by electroplating with a commercial solution on the above thick photoresist substrate (Fig. 1(i)).

### 2.2. Bump formation

The next step is the deposition of Sn–Ag by electropla-

† Corresponding author. Email: leluo@mail.sim.ac.cn

Received 3 January 2011, revised manuscript received 28 March 2011

© 2011 Chinese Institute of Electronics

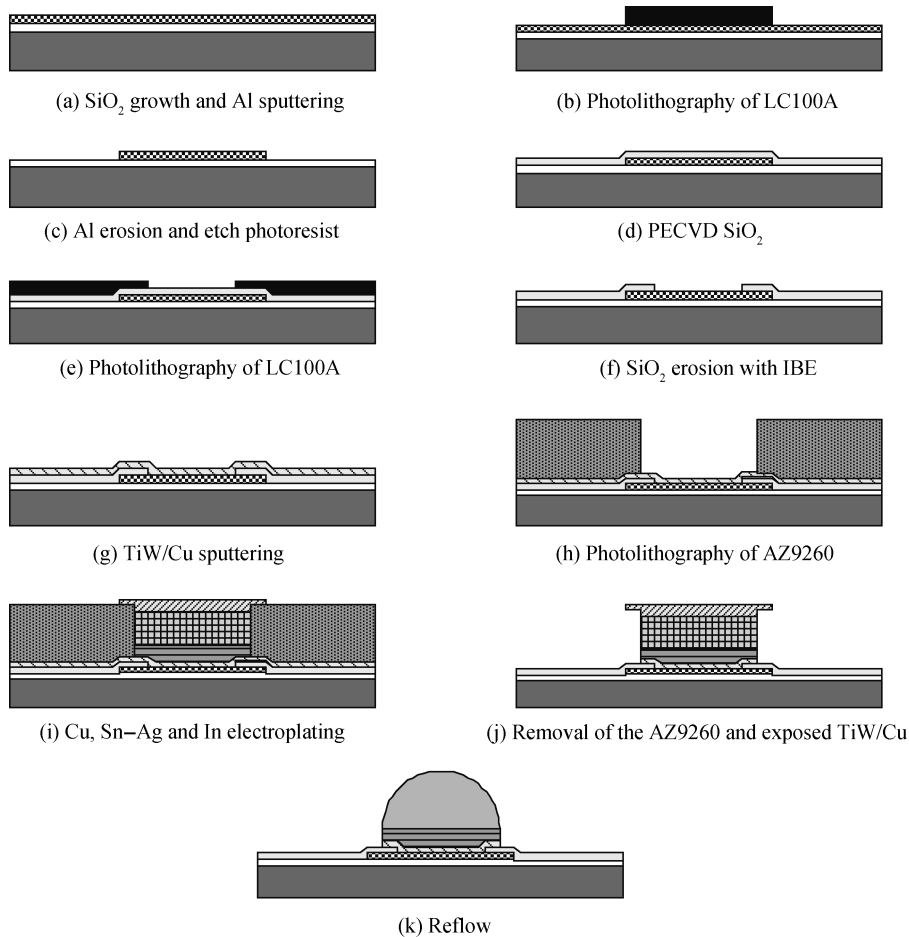


Fig. 1. Flow chart of Sn-Ag-In solder bumping process.

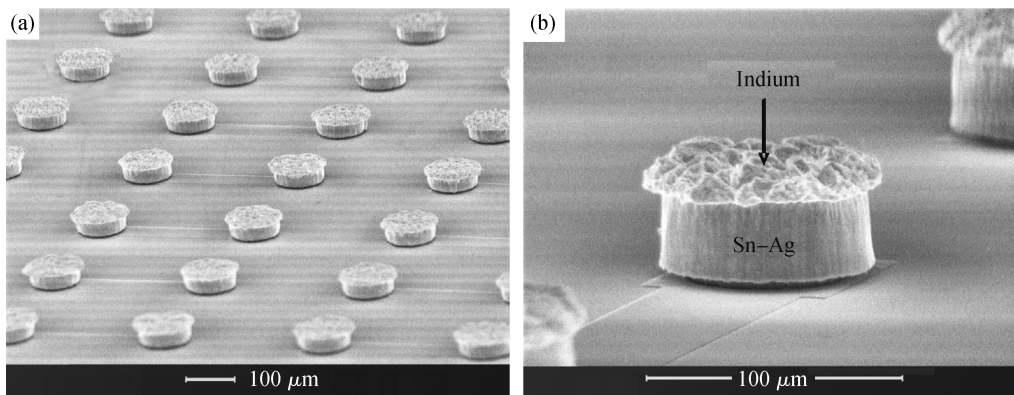


Fig. 2. SEM pictures of Sn-Ag-In mushrooms achieved after electroplating.

ting on Cu UBM. Electroplating was performed in SLO-TOLOY SNA30 solution with pure Sn (99.95%) as the anode. The plating rate was about 8 μm/h at 25 °C with a current density of 20 mA/cm<sup>2</sup>. The thickness of tin-silver was controlled to 40–41 μm. After that, indium electroplating was performed in an indium sulfamate plating bath at room temperature. The bath comprised In(NH<sub>2</sub>SO<sub>3</sub>)<sub>3</sub> 105.36 g/L, NaNH<sub>2</sub>SO<sub>3</sub> 150 g/L, HNH<sub>2</sub>SO<sub>3</sub> 26.4 g/L, NaCl 45.84 g/L, dextrose 8 g/L and triethanolamine 2.29 g/L with pH 1.5–2. Indium with 99.999% purity was used as the anode. The thickness of indium was controlled to 4–5 μm. Then the AZ9260 photoresist and the ex-

posed TiW/Cu were etched away in sequence (Fig. 1(j)). Figure 2 shows the Sn-Ag-In mushrooms obtained at the end of the bump formation phase.

### 2.3. Reflow

The reflow (Fig. 1(k)) was performed in a five-zone Falcon 8500 oven in N<sub>2</sub> atmosphere. The temperature of each zone was 80, 160, 200, 260 and 80 °C, respectively. The soaking time was 30 s in each zone and the transport time to the next zone was about 15 s. Some samples were reflowed at 260 °C for

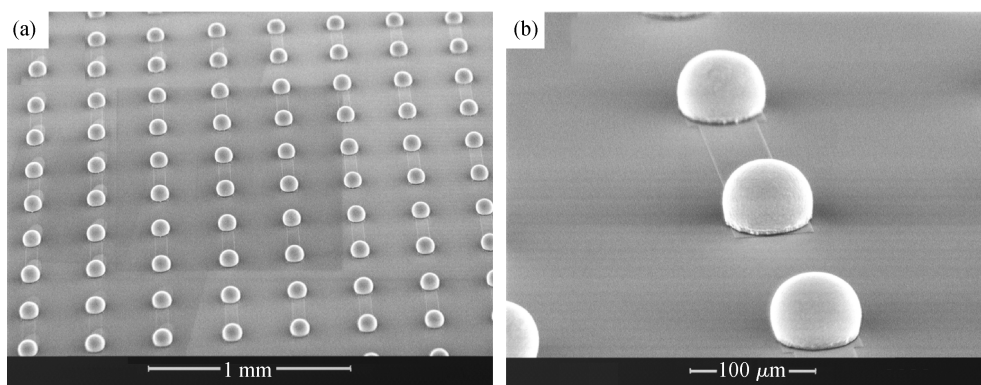


Fig. 3. SEM pictures of Sn–Ag–In solder bumps with a reflow at 260 °C for 30 s.

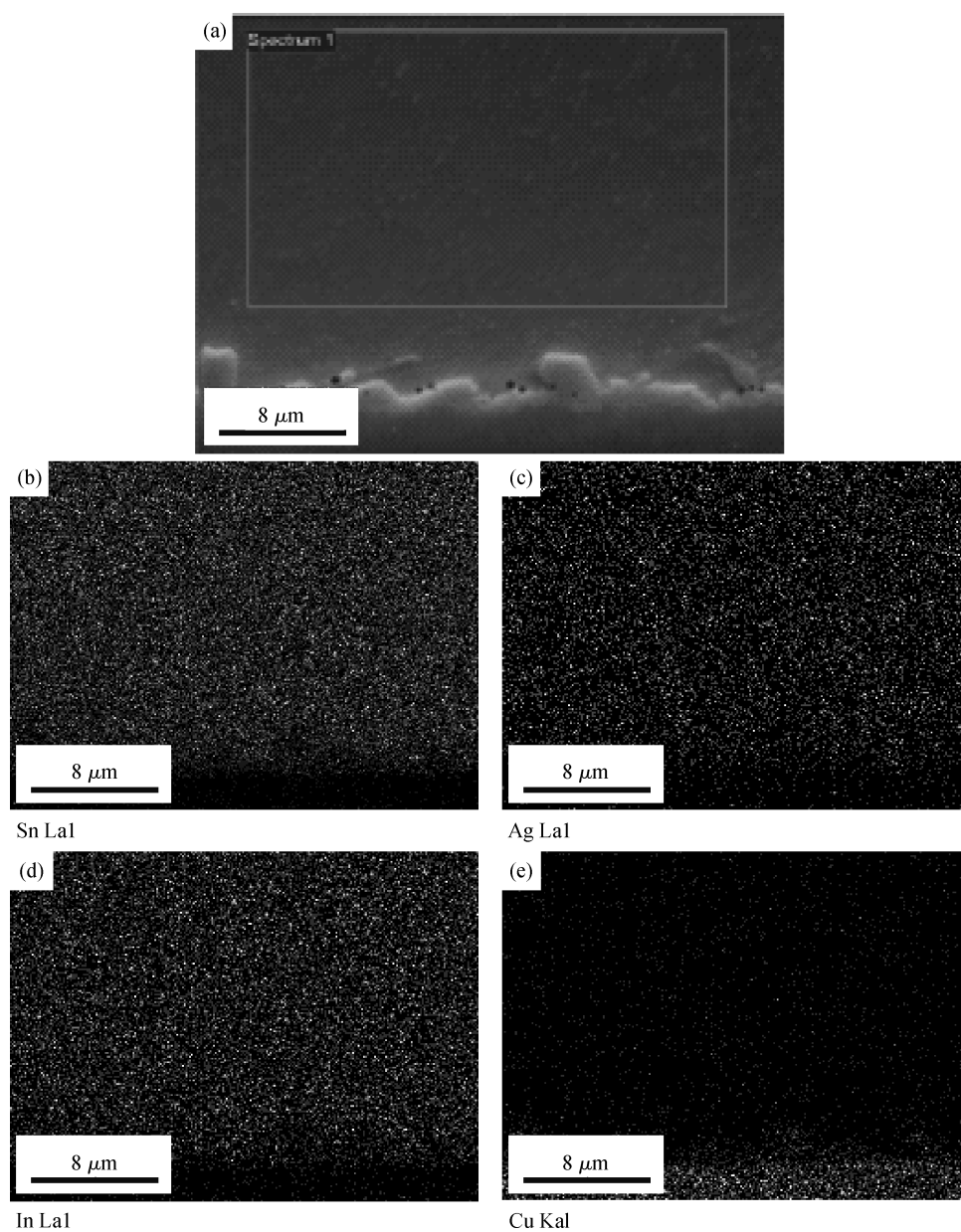


Fig. 4. Cross-sectional EPMA maps of Sn–Ag–In solder bump with a reflow at 260 °C for 30 s. (a) SEM image of the cross-section. (b) Map of Sn. (c) Map of Ag. (d) Map of In. (e) Map of Cu.

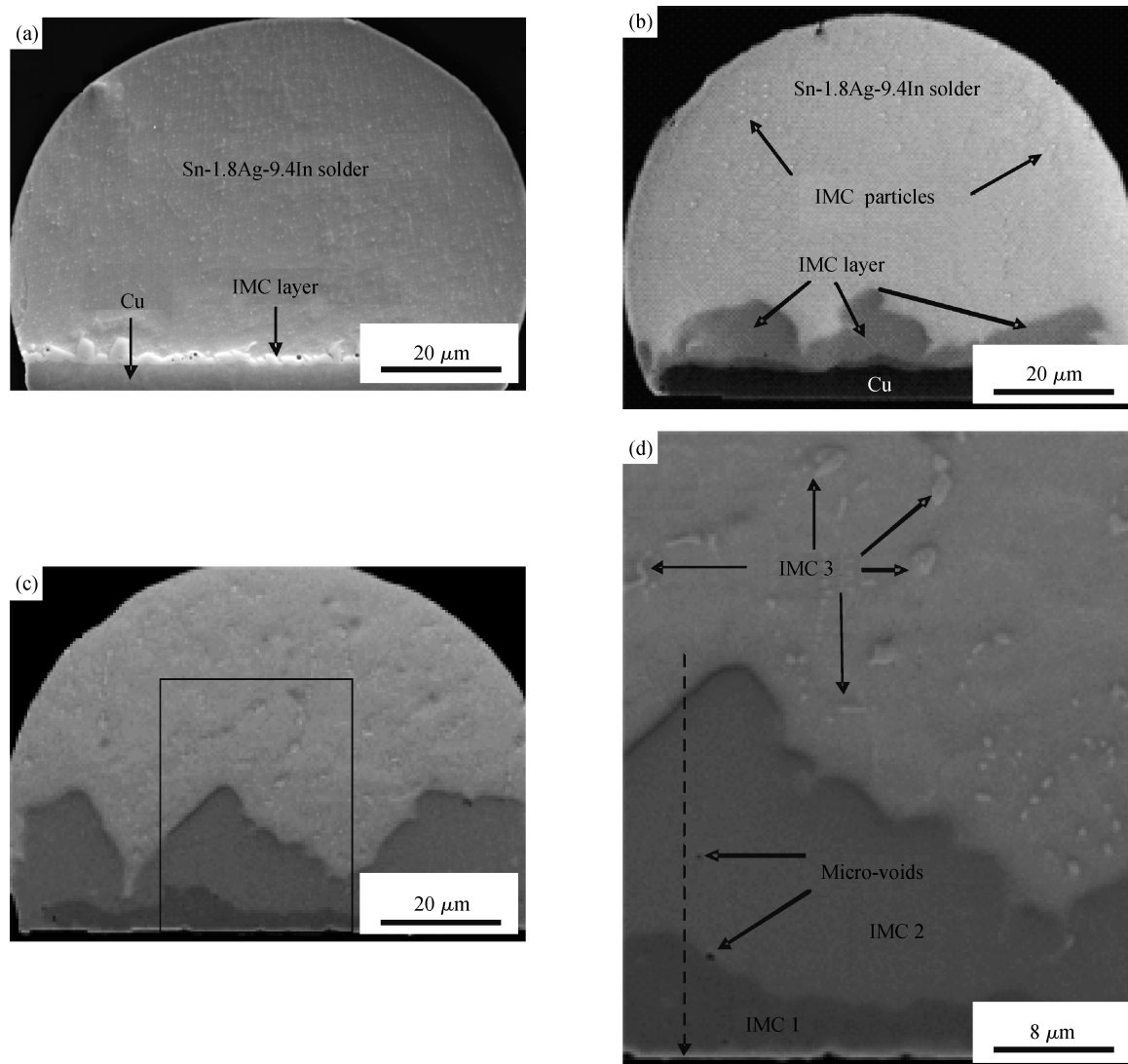


Fig. 5. Cross-sectional SEM micrographs of a Sn-1.8Ag-9.4In solder bump with a reflow at 260 °C for (a) 30 s, (b) 10 min and (c) 30 min. (d) High magnification view of the rectangular region in (c).

30 min for the purpose of observing IMCs between Sn-Ag-In solder and Cu.

The microstructure of the interfacial reaction region between the solder and Cu was investigated by cross-sectional scanning electron microscopy (SEM) equipped on electron probe microanalysis (EPMA). Energy dispersive X-ray spectroscopy (EDX) was used to determine the phase composition. SEM samples were prepared by a standard cross-sectioning method.

The shear test of the solder bumps was conducted on Dage 4000 equipment. The shear height and speed was 20  $\mu\text{m}$  and 100  $\mu\text{m/s}$ , respectively. At least 25 bumps were measured for each compo ternary alloy. The variation in shear strength was analyzed statistically<sup>[18]</sup>.

### 3. Results and discussion

Figure 3 shows a view of the obtained solder bumps. It can be seen that the Sn-Ag-In solder bumps have well-controlled geometry and smooth shiny surfaces, and the diameter and

pitch of the solder bump are about 70  $\mu\text{m}$  and 320  $\mu\text{m}$ , respectively.

Figure 4 shows the EPMA maps of the cross-section of a Sn-Ag-In solder bump with a reflow at 260 °C for 30 s. The maps of different elements indicate that the Sn, Ag and In are almost uniformly distributed in the solder bumps, except that some segregation in the local area. So it can be concluded that tin-silver and indium mixes well during the reflow process. EDX area scanning from the rectangular region in Fig. 4(a) is applied to analyze the solder composition. The result shows that the composition (wt.%) of the Sn-Ag-In solder bump is Sn : Ag : In = 89.19 : 1.67 : 9.14. After being converted into atomic percentages, the ternary solder can be rewritten as  $\text{Sn}_{1.8}\text{Ag}_{9.4}\text{In}$ .

Figure 5 shows the cross-sectional SEM micrographs of a Sn-Ag-In solder bump with a reflow at 260 °C for different times. According to microstructural observation, the IMCs between Sn-Ag-In solder and Cu grow with the reflow time. On the other hand, Cu is consumed rapidly during the liquid/solid interfacial reaction. After 30 min reflow, rare Cu is left. Three

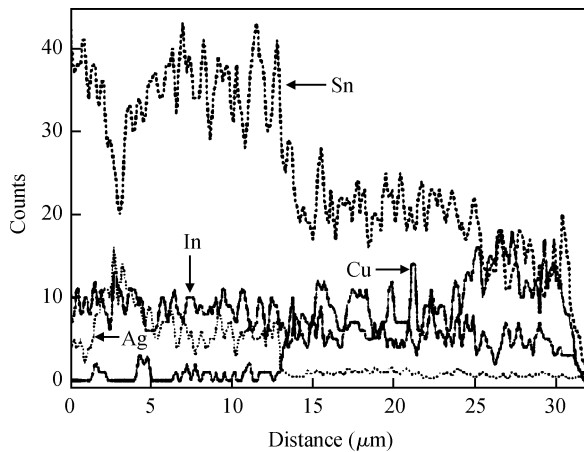


Fig. 6. Elemental distribution along the dashed line in Fig. 5(d).

Table 1. EDS results of the indicated IMC phases in Fig. 5(d).

IMC	IMC composition at.%	Phase identification
1	Cu: 74.7 Sn: 23.35 In: 1.95	$Cu_3(Sn_{0.92}In_{0.08})$
2	Cu: 53.33 Sn: 43.72 In: 2.95	$Cu_6(Sn_{0.94}In_{0.06})_5$
3	Ag: 64.43 In: 35.57	$Ag_2In$

kinds of IMCs are observed in the Sn–Ag–In/Cu system: IMC 1 and IMC 2, which are formed at the Sn–Ag–In/Cu interface, and IMC 3, the small particles dispersing in the Sn–Ag–In solder matrix. The compositions of various IMCs are shown in Table 1. According to the EDX results, the thinner and smoother IMC layer near the Cu side is  $Cu_3(Sn_{0.92}In_{0.08})$ , which is based on  $Cu_3Sn$ . The thicker and rougher IMC layer near the Sn–Ag–In solder side is  $Cu_6(Sn_{0.94}In_{0.06})_5$ , which is based on  $Cu_6Sn_5$ . And the small IMC particles dispersing in the solder matrix are  $Ag_2In$ . The presence of indium in IMC layers between Sn–Ag–In solder and Cu indicates the interdiffusion of Sn, In and Cu atoms during reflow, which is also confirmed by the line scanning along the dashed line in Fig. 5(d) (just as Figure 6 shows). Micro-voids are observed at the  $Cu_3(Sn_{0.92}In_{0.08})/Cu_6(Sn_{0.94}In_{0.06})_5$  interface, and some appear in the  $Cu_6(Sn_{0.94}In_{0.06})_5$  phase (see the arrows in Fig. 5(d)). The former are Kirkendall voids, which are due to the interdiffusion between different element species during the interfacial reaction<sup>[19]</sup>. Because of the limited evidence, the formation of voids in  $Cu_6(Sn_{0.94}In_{0.06})_5$  phase needs further investigation.

Figure 7 shows the SEM images of the fracture surfaces of solder bumps with different reflow time after shear testing. The fracture surfaces exhibit mainly a ductile failure, but with little brittle failure from the  $Cu_6(Sn_{0.94}In_{0.06})_5$  IMC around the bump edges. The tendency towards a brittle IMC fracture is also intensified with increasing reflow time, as shown in Figs. 7(b) and 7(c). Figure 8 shows the curves of cumulative probability of the shear strength of solder bumps reflowed for different times. From the coefficients of the linear fitting (the value of *R* is close to 1.0), it can be concluded that the data sets statistically follow the normal distribution. Comparison of *R* values shows that for different reflow times, the shear strength of solder bumps with a reflow time of 30 s appears to follow the ideal normal distribution somewhat better than

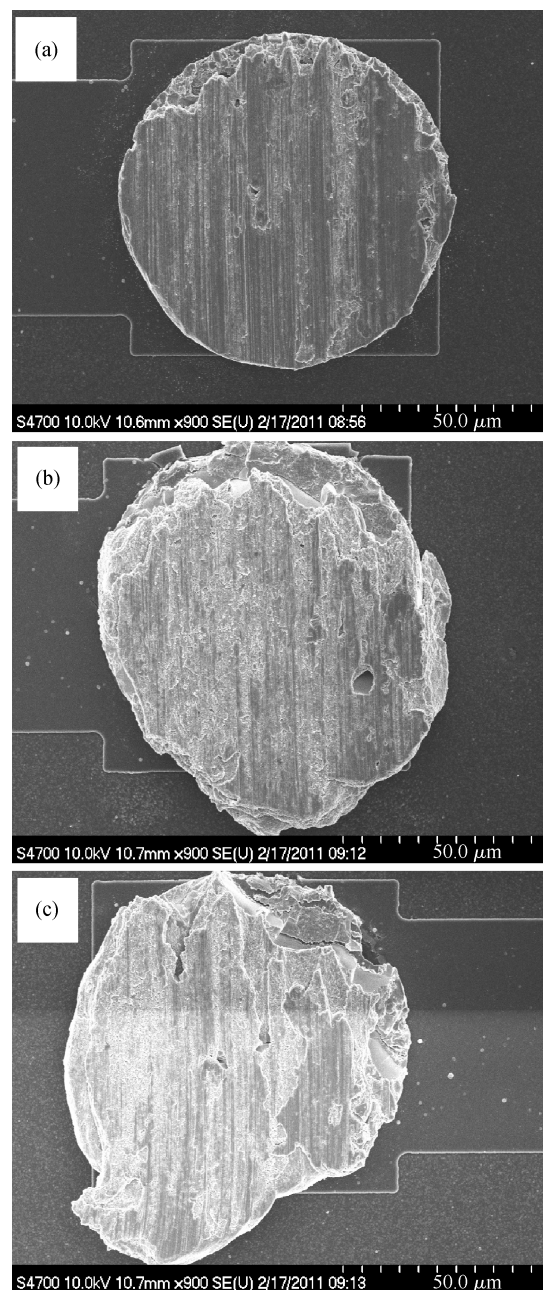


Fig. 7. Typical SEM shear fracture surfaces of Sn–Ag–In solder bumps with a reflow at 260 °C for (a) 30 s, (b) 10 min and (c) 30 min.

that of solder bumps with a reflow time of 10 min and 30 min. This is due to the fact that for 30 s reflow, almost only the solder matrix determines the shear strength (Fig. 7(a)), but for 10 and 30 min reflow, the effect of  $Cu_6(Sn_{0.94}In_{0.06})_5$  IMC is more obvious, which increases the complexity of the influencing factor. The mean shear strength can be calculated as 103 MPa, 117 MPa and 126 MPa for solder bumps with reflow for 30 s, 10 min and 30 min, respectively. Correspondingly, the standard deviation of shear strength is 8.9, 9.8 and 17.7 MPa, respectively. The mean shear strength of the solder bumps increases with reflow time, which indicates the following fact: the growth of IMC layers will consume Sn–In from solder matrix, which results in an increase in Ag concentration in the solder area. So during solidification, more  $Ag_2In$  will nucleate

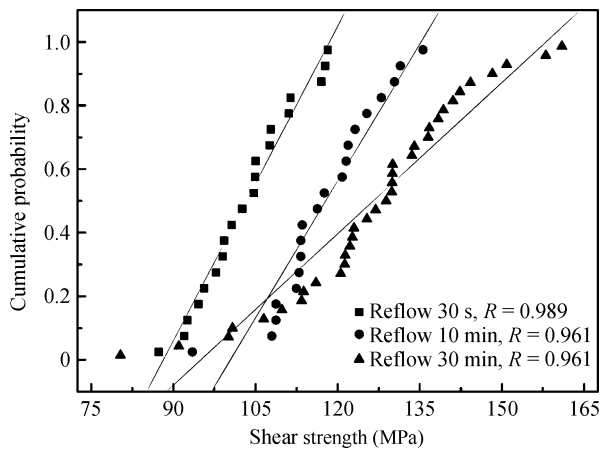


Fig. 8. Cumulative probability curves of the shear strength of solder bumps with a reflow at 260 °C for different times on the normal coordinates.

and strengthen the solder. On the other hand, the growth and coarsening of  $\text{Cu}_6(\text{Sn}_{0.94}\text{In}_{0.06})_5$  increases the joint area with increasing reflow time, thereby improving the shear strength. However, because of the small fraction of brittle fracture from  $\text{Cu}_6(\text{Sn}_{0.94}\text{In}_{0.06})_5$  IMC, the later factor is subordinate.

#### 4. Conclusions

A new technique to make Sn–Ag–In ternary solder bumps in fine pitch is presented. With this technique,  $\text{Sn}_{1.8}\text{Ag}_{9.4}\text{In}$  solder bumps are obtained by electroplating Sn–Ag and indium in sequence. After reflow at 260 °C for 30 s, Sn, Ag and In are uniformly distributed. It is found that the intermetallic compounds between Sn–Ag–In solder and Cu grow with the reflow time, which results in an increase in Ag concentration in the solder area. So during solidification, more  $\text{Ag}_2\text{In}$  nucleates and strengthens the solder. There are a lot of applications of this flip chip technique to satisfy the huge commercial interest in high density packaging. One example is the fabrication of pixel systems where low pitch and very large numbers of bumps are needed. Furthermore, there is also interest in fields such as MCMs and microsystems.

#### References

- [1] Huang M L, Wang L, Wu C M L. Creep behavior of eutectic Sn–Ag lead-free solder alloy. *Journal of Materials Research*, 2002, 17: 2897
- [2] Kariya Y, Otsuka M. Mechanical fatigue characteristics of Sn–3.5Ag–X (X = Bi, Cu, Zn and In) solder alloys. *J Electron Mater*, 1998, 27(11): 1229
- [3] Yeh M S. Effects of indium on the mechanical properties of ternary Sn–In–Ag solders. *Metallurgical and Materials Transactions A*, 2003, 34(2): 361
- [4] Huang M L, Wang L. Effects of Cu, Bi, and In on microstructure and tensile properties of Sn–Ag–X (Cu, Bi, In) solders. *Metallurgical and Materials Transactions A*, 2005, 36(6): 1439
- [5] Anderson I E, Cook B A, Harringa J L, et al. Microstructural modifications and properties of Sn–Ag–Cu solder joints induced by alloying. *J Electron Mater*, 2002, 31(11): 1166
- [6] Ohnuma I, Miyashita M, Liu X J, et al. Phase equilibria and thermodynamic properties of Sn–Ag based Pb-free solder alloys. *IEEE Trans Electron Packag Manuf*, 2003, 26(1): 84
- [7] Mei Z, Morris J W. Superplastic creep of low melting point solder joints. *J Electron Mater*, 1992, 21(4): 401
- [8] Wang P J, Kim J S, Lee C C. Intermetallic reaction between electroplated indium and silver layers. *59th Electronic Components and Technology Conference*, 2009: 1317
- [9] Yu A M, Lee C W, Kim M S, et al. The effect of the addition of In on the reaction and mechanical properties of Sn–1.0Ag–0.5Cu solder alloy. *Metals and Materials International*, 2007, 13(6): 517
- [10] Yoon J W, Chun H S, Jung S B. Correlation between interfacial reactions and shear strengths of Sn–Ag–(Cu and Bi–In)/ENIG plated Cu solder joints. *Mater Sci Eng A*, 2008, 483/484: 731
- [11] Chen Y C, So W W, Lee C C. A fluxless bonding technology using indium–silver multilayer composites. *IEEE Trans Compon, Packag, and Manuf Technol*, 1997, 20(1): 46
- [12] Cheng M D, Chang S Y, Yen S F, et al. Intermetallic compounds formed during the reflow and aging of Sn–3.8Ag–0.7Cu and Sn–20In–2Ag–0.5Cu solder ball grid array packages. *J Electron Mater*, 2004, 33(3): 171
- [13] Sharif A, Chan Y C. Interfacial reactions on electrolytic Ni and electroless Ni(P) metallization with Sn–In–Ag–Cu solder. *Journal of Alloys and Compounds*, 2005, 393: 135
- [14] Sharif A, Chan Y C. Effect of indium addition in Sn-rich solder on the dissolution of Cu metallization. *Journal of Alloys and Compounds*, 2005, 390: 67
- [15] Huang Q P, Xu G W, Yuan Y, et al. Development of indium bumping technology through AZ9260 resist electroplating. *J Microelectron Microeng*, 2010, 20: 055035
- [16] Ha S S, Jang J K, Ha S O, et al. Effect of multiple reflows on interfacial reaction and shear strength of Sn–Ag electroplated solder bumps for flip chip package. *Microelectron Eng*, 2010, 87(3): 517
- [17] Chao P S, Huang J T, Hsu H J, et al. Fabrication on uniform plating-based flip chip solder bumps after reflow process using a polishing mechanism. *Microelectron Eng*, 2007, 84(1): 60
- [18] Li J F, Mannan S H, Clode M P, et al. Dissolution and interfacial reaction of Nb in contact with the molten 52In–48Sn solder. *Acta Materialia*, 2007, 55: 5057
- [19] Liu C Y, Tu K N, Sheng T T, et al. Electron microscopy study of interfacial reaction between eutectic SnPb and Cu/Ni(V)/Al thin film metallization. *J Appl Phys*, 2000, 87: 750